A New Variational Model for Segmentation and Denoising of Images with Multiplicative Noise ☆,☆☆

Iulia Posirca[a,∗], Yunmei Chen[b], Celia Z. Barcelos[c]

[a]*Department of Mathematics, Santa Fe College, Gainesville, FL 32606 Tel: (352) 395-5093 Ext 6306*
[b]*Department of Mathematics, University of Florida, Gainesville, FL 32611 Tel: (352) 392-0281 Ext 268 Fax: (352) 392-8357*
[c]*Departamento de Matemática, Universidade Federal de Uberlandia, Uberlandia, Brazil Tel: (34) 32394156*

Abstract

In this paper, we develop a variational model for simultaneous multiphase segmentation and denoising of images corrupted with multiplicative noise. The presented model uses soft segmentation, which allows each pixel to belong to each image pattern with some probability being more flexible than the classical hard segmentation. The denoising is performed by minimizing a variable exponential growth functional, which is a combination between TV-based and isotropic smoothing for better feature preserving. The model development and computational implementation are explored in detail, and experimental results on real and synthetic images are presented.

Keywords: multiplicative noise, soft segmentation, variable exponential growth energy functional.

---

1. Introduction

Noise removal and image segmentation are two key steps in image vision modelling and analysis. Multiplicative denoising problems have received more attention in the recent years [1,8,11-13,16,17,24]. In a multiplicative noise model, a given image I defined on a rectangle $\Omega \subset R^2$, is the multiplication

---

of an original image u and a noise n:

$$I = un.$$

Without loss of generality, we can assume that u and n are positive in the noise model. It is well known that multiplicative noises are found in many real world image processing applications, such as SAR images, laser images and medical ultrasonic images. Unlike additive noises, the multiplicative ones are more difficult to be removed from the corrupted images because of their multiplicative nature. The additive noise removal problems, such as the PDE-based variational methods, have been studied extensively over the last decades. These include the Rudin-Osher-Fatemi (ROF) model [22] and Lysaker-Lundervold-Tai (LLT) model [18]. Given a noisy image $I = u + n$, the ROF model can be described as the minimization of the functional

$$\int_\Omega |\nabla u| + \int_\Omega \alpha(u - I)^2. \tag{1.1}$$

The first term of the functional is the TV-regularization term and the second is the fitting term with α as the weighted parameter. This model preserves well the sharp edges in image denoising and it was used extensively for images corrupted with additive gaussian noise.

In comparison to the additive noise, the multiplicative noise removal has not yet been studied completely. As we know so far, the variational approach was proposed firstly by Rudin, Lions and Osher (RLO model)[23] as the minimization of the energy functional

$$E(u) = \alpha \int_\Omega |\nabla u| + \alpha_1 \int_\Omega \frac{I}{u} + \alpha_2 \int_\Omega (\frac{I}{u} - 1)^2 \tag{1.2}$$

where $I = un$ is the image contaminated with multiplicative noise and the last two terms are the data fitting terms with α_1, α_2 the weighted parameters. Recently, several variational approaches are devoted to the multiplicative noise removal [1,8,10-13,16].

An important model, which can be applied to the non-textured SAR images, is the variational model proposed by Aubert and Aujol (AA model) [1]. The authors proposed the following restoration model

$$inf_u \int_\Omega |\nabla u| + \lambda \int_\Omega (logu + \frac{I}{u}) \tag{1.3}$$

where u belongs to $BV(\Omega)$, $u > 0$, $I = un$, $I > 0$ in $L^\infty(\Omega)$ is the observed noisy image and λ is a regularization parameter. The (AA) model is specifically devoted to the denoising of images corrupted by Gamma noise, which appears more frequently in SAR images. The authors proved the existence of a minimizer for the problem (1.3).

Motivated by the (AA) model, the authors in papers [11] developed the following denoising model:

$$min_u \int_\Omega |\nabla u| + \lambda \int_\Omega (u + Ie^{-u}). \tag{1.4}$$

The new fitting term $u + Ie^{-u}$ is obtained from the fitting term $logu + \frac{I}{u}$ used in the (AA) model, under the exponential transformation: $u \to e^u$. The authors [11] motivation is that the new fitting term image $u + Ie^{-u}$ becomes globally convex for all u and $I > 0$, which ensures the uniqueness of the solutions to the variational problem (1.4). In plus, the proposed fitting term preserves well the image edges.

Another variational model for multiplicative noise removal was developed in paper [13]. This model was motivated by the form of the corrupted image (for instance in medical ultrasound images)

$$I = u + \sqrt{u}n \tag{1.5}$$

where n is a zero mean Gaussian variable. In their work, the authors introduced the following fitting term for removing the "speckle" noise in the ultrasound images:

$$E_1(u) = \int_\Omega \frac{(I - u)^2}{u}. \tag{1.6}$$

The restoration model of the noiseless image u becomes

$$min_u \int_\Omega |\nabla u| + \lambda \int_\Omega \frac{(I - u)^2}{u}. \tag{1.7}$$

The model was implemented with good results.

The segmentation of images with additive Gaussian noise has been studied extensively and many models have been developed with various methods (e.g. [2-7,14,15,19,20,21,26,27]). However, the segmentation of images corrupted with multiplicative noise is more challenging in many cases. For instance, the medical ultrasound images are difficult to be segmented because of low signal/noise ratio which reduces greatly the observable details in such images. Consequently, the accuracy and precision of the measurements are compromised. In the recent years, more attention has been paid to tackle this problem. For instance, in the work of [10,17,24], several models have been developed for segmenting images contaminated with multiplicative noise. The models developed in [17] concerns the piecewise constant segmentation, where the authors proposed the following variational framework:

Let $u_0 : \Omega \to R$, $u_0 = un$ be an observed image containing the multiplicative noise n and the domain Ω is bounded with Lipschitz boundary. Assume that u is piecewise constant. Denote by C included in Ω the contour which separates Ω into two regions Ω_1 and Ω_2, and let the Lipschitz function ϕ be a level set function which represent C. Then the functional energy for the two-phase case segmentation is given by

$$L(c_1, c_2, \phi) = \lambda_1 \int_\Omega (u_0/c_1 - 1)^2 + \lambda_2 \int_\Omega (u_0/c_2 - 1)^2 + \mu \int_\Omega |\nabla H(\phi)|. \tag{1.8}$$

The energy minimization problem is solved using the Euler-Lagrange equation for the unknown level set function ϕ, and c_1, c_2.

3

Due to the fact that ultrasound images have poor signal to noise ratio and higher inhomogeneity, the piecewise constant Mumford-Shah model presented in [17] is not efficient for segmentation of images with multiplicative noise.

In [24], a region based active contour model is developed using MLE with the assumption that the image intensity at each pixels is an independent random variable with Rayleigh distribution. A finite difference approximation for the curve evolution was derived. The models presented in [17,24] were tested on real (ultrasound) and synthetic images.

In this work we will present a novel variational framework for simultaneous denoising and multiphase segmentation of the images corrupted with multiplicative noise. The segmentation is performed by estimating the probabilities that each pixel belongs to the partitioned sub-regions. The denoising is carried out by minimizing a variable exponential growth functional, which consists of a combination of TV-based and isotropic smoothing, and a data fitting term under the consideration of multiplicative noise. The model development and computational implementation are explored in section 2 and 3 respectively, and experimental results and comparisons with existing models on real and synthetic images are presented in section 4. We present our conclusions on the proposed work in section 5.

2. Proposed work

In this section, we will make a more detailed presentation of our proposed variational model for simultaneous noise removal and multiphase segmentation of images contaminated with multiplicative noise. Let $I : \Omega \to R$ be a noisy image defined on an open, bounded, smooth domain $\Omega \subset R^2$. Suppose that the image I has K patterns and it can be modeled as corrupted with noise of the form (1.5).

The proposed model refers to the minimization of an energy functional which contains two parts: the noise removal and, respectively the soft segmentation part. First, we denote by $u_i(x)$ the mean field of the intensity of the pattern i and $p_i(x)$ the probability that the pixel x from Ω belongs to the pattern i, satisfying the simplex constraints

$$\sum_{i=1}^{K} p_i(x) = 1, 0 \le p_i(x) \le 1, i = 1, ..., K. \tag{2.1}$$

Then, for our work, the noise can be modeled by the formula:

$$n^2(x) = \sum_{i=1}^{K} \frac{(I(x) - u_i(x))^2 p_i(x)}{u_i(x)} \tag{2.2}$$

for any x from Ω.

The proposed model for simultaneous denoising and soft segmentation of the images corrupted with "speckle" noise refers to the minimization of the following

4

energy functional:

$$E[p_i, u_i|I] = \alpha \sum_{i=1}^{K} \int_{\Omega} |\nabla u_i(x)|^{q(x)} + \lambda \sum_{i=1}^{K} \int_{\Omega} \frac{(I(x) - u_i(x))^2 p_i(x)}{u_i(x)}$$

$$+ \sum_{i=1}^{K} \int_{\Omega} |\nabla p_i(x)|^2 + \int_{\Omega} (\sum_{i=1}^{K} \sqrt{p_i(x)})^2, i = 1, ..., K \qquad (2.3)$$

where α and λ are weighted parameters and the memberships functions $p_i(x)$ are subject to the simplex constraints (2.1).

The reconstructed image result for the proposed model at any pixel x from Ω is given by the formula

$$u(x) = \sum_{i=1}^{K} u_i(x) p_i(x). \qquad (2.4)$$

In the proposed work, the smoothing part of the energy functional contains a variable exponent defined as

$$q(x) = \begin{cases} 1 + \frac{1}{1+\beta|\nabla G_{\tilde{\sigma}} * I(x)|^2}, & if |\nabla u(x)| \leq \rho \\ 1, & if |\nabla u(x)| > \rho \end{cases} \qquad (2.5)$$

with $\beta, \rho > 0$ fixed, and $G_{\tilde{\sigma}}$ a Gaussian function.

Using this functional with variable exponent will give the model the following benefits:

a) it ensures TV based diffusion ($q(x) = 1$) along edges and Gaussian smoothing ($q(x) = 2$) in homogenous regions and,

b) it employs anisotropic diffusion ($1 < q(x) < 2$) in regions in which the difference between noise and edge is difficult to distinguish.

For our work model, we also seek to minimize the term

$$\sum_{i=1}^{K} \int_{\Omega} |\nabla p_i(x)|^2 + \int_{\Omega} (\sum_{i=1}^{K} \sqrt{p_i(x)})^2. \qquad (2.6)$$

That means, we impose the condition that membership functions $p_i(x)$ are smooth inside the pattern and discontinuous across it.

Denote by $P = (p_1, ..., p_K)$ the membership probability defined on the $(K-1)$-simplex. In plus, for any x from Ω, the membership P is forced to be close to the vertices of the (K-1) simplex, i.e. each $p_i(x)$ is close to either 0 or 1, for $i = 1, 2, ..., K$.

To find an optimal solution for the minimization of the energy functional (2.3), we compute the Euler-Lagrange equations associated with this problem. Denote $U = (u_1, ..., u_K)$ with the membership $P = (p_1, ..., p_K)$.

The first order variation of the energy functional given by (2.3) with respect to the membership P is computed by using the projection on (K-1)simplex technique [21,25].

We can write the equations for the first order variation of the energy E with respect to P without the simplex constraints (2.1) as

$$\partial E = \int_\Omega \sum_{i=1}^K W_i \delta p_i dx + \int_{\partial\Omega} \sum_{i=1}^K w_i \delta p_i dH, \qquad (2.7)$$

where H is the Hausdorff measure on $\partial\Omega$ and

$$W_i = -\Delta p_i(x) + \lambda \frac{(I(x) - u_i(x))^2}{u_i(x)} + \frac{1}{K} \frac{\sum_{i=1}^K \sqrt{p_i}}{\sqrt{p_i}}, x \in \Omega, \qquad (2.8)$$

$$w_i = \frac{\partial p_i(x)}{\partial n}, x \in \partial\Omega. \qquad (2.9)$$

Taking $W = (W_1, ..., W_K)$ and $w = (w_1, ..., w_K)$, the relation (2.7) can be written in the free-gradient form

$$\frac{\partial E}{\partial_f P} = W|_\Omega + w|_{\partial\Omega}. \qquad (2.10)$$

Because P belongs to the $(K-1)$-simplex, we consider the orthogonal projection

$$\Pi : T_P R^K \to T_P \Delta_{K-1}.$$

For any $t \in T_P R^K$,

$$\Pi(t) = t - \frac{1_K <t, 1_K>}{K} = t- <t> 1_K,$$

where $<t> = \frac{\sum_{i=1}^K t_i}{K}$ and $\frac{1_K}{\sqrt{K}} = \frac{(1,...,1)}{\sqrt{K}}$ is the normal direction of the tangent plane.

The constrained gradient of E on the $(K-1)$-simplex is given by

$$\frac{\partial E}{\partial P} = \Pi(\frac{\partial E}{\partial_f P}) = (W- <W> 1_K)|_\Omega + (w- <w> 1_K)|_{\partial\Omega}. \qquad (2.11)$$

To solve the equation

$$\frac{\partial E}{\partial P} = 0 \qquad (2.12)$$

is equivalent to solve the Euler- Lagrange system of equations on P, given U:

$$W_i(x) = <W(x)>, x \in \Omega, \qquad (2.13)$$

$$w_i(x) = <w(x)>, x \in \partial\Omega \qquad (2.14)$$

where W_i and w_i are given in the relations (2.8) and (2.9).

The Euler- Lagrange system of equations on U, given P is

$$\alpha \, div(q(x)|\nabla u_i(x)|^{q(x)-2}\nabla u_i(x)) + \lambda(\frac{I(x)^2}{u_i(x)^2} - 1)p_i(x) = 0, x \in \Omega, \qquad (2.15)$$

$$q(x)|\nabla u_i(x)|^{q(x)-2}\frac{\partial u_i(x)}{\partial n} = 0, x \in \partial\Omega. \qquad (2.16)$$

6

3. Algorithm

To obtain an optimal solution $(\mathbf{U},\mathbf{P})$ to problem (2.3), we used the alternating minimization (AM) algorithm. For each step $(n+1)$, given the patterns $\mathbf{U}^n = (u_i^n; i = 1, 2, ..., K)$ and the ownership $\mathbf{P}^n = (p_i^n; i = 1, 2, ..., K)$ find

$$\mathbf{P}^{n+1} = argmin_{\mathbf{P}} E[\mathbf{P}|\mathbf{U}^n, I] \qquad (3.1)$$

where $\mathbf{U}=(u_1, ..., u_K)$ and $\mathbf{P}=(p_1, ..., p_K)$ satisfies the simplex constraints (2.1).

To find a solution of the equation (2.12) is equivalent to solve the associated flow equation:

$$\frac{d(p_i)}{dt} = L_{p_i}(I, u_i, p_i,) \qquad (3.2)$$

where

$$L_{p_i}(I, u_i, p_i) = W_i - <W> \qquad (3.3)$$

with W_i defined in (2.8) and $<W> = \frac{\sum_{i=1}^{K} W_i}{K}$.

Therefore

$$L_{p_i}(I, u_i, p_i) = \lambda \frac{(I - u_i)^2}{u_i} - \Delta p_i + \frac{1}{K} \frac{\sum_{i=1}^{K} \sqrt{p_i}}{\sqrt{p_i}} - <W> \qquad (3.4)$$

and

$$<W> = \frac{1}{K} \sum_{i=1}^{K} \left(-\Delta p_i + \lambda \frac{(I - u_i)^2}{u_i} + \frac{1}{K} \frac{\sum_{i=1}^{K} \sqrt{p_i}}{\sqrt{p_i}} \right)$$

$$= \frac{1}{K} \sum_{i=1}^{K} \left(\lambda \frac{(I - u_i)^2}{u_i} + \frac{1}{K} \frac{\sum_{i=1}^{K} \sqrt{p_i}}{\sqrt{p_i}} \right) \qquad (3.5)$$

since

$$\Delta \left(\sum_{i=1}^{K} p_i \right) = 0. \qquad (3.6)$$

Following, given $\mathbf{P}^n$ and $\mathbf{U}^n$,

$$\mathbf{U}^{n+1} = argmin_{\mathbf{U}} E[\mathbf{U}|\mathbf{P}^n, I] \qquad (3.7)$$

which is equivalent to solving the associated flow equation

$$\frac{d(u_i)}{dt} = L_{u_i}(I, u_i, p_i,) \qquad (3.8)$$

where

$$L_{u_i} = \alpha \ div(q|\nabla u_i|^{q-2}\nabla u_i) + \lambda \left(\frac{I^2}{u_i^2} - 1 \right) p_i \qquad (3.9)$$

and q (depending on x) is given in relation (2.5).

Summarizing, the updating...$(\mathbf{U^n}, \mathbf{P^n})... \to (\mathbf{U}^{n+1}, \mathbf{P}^{n+1})...$ is obtained solving the following system of equations:

$$p_i^{n+1} = p_i^n + dt_p L_{p_i}(I, u_i^n, p_i^n),$$
$$u_i^{n+1} = u_i^n + dt_u L_{u_i}(I, u_i^n, p_i^n). \qquad (3.10)$$

where dt_p and dt_u are steps sizes, L_{p_i}, L_{u_i} are defined in (3.4) and (3.9).

7

4. Experiments

To show the effectiveness of our model, six experiments were performed. For all experiments, the contaminated image I is given by the formula (1.5). Denote by n the number of iterations for each experiment.

Figure 1 is a comparison between the RLO model (1.2) and the proposed model (2.3) using a synthetic image contaminated with multiplicative noise. Figure 1(a) is the original clean image, figure 1(b) is the contaminated image with multiplicative Gaussian noise of mean zero and variance 0.03. Figure 1(c)-(d) represent the reconstructed image result $u(x)$ using our model, respectively the RLO model. We have tested the performance of our model by computing the signal to noise ratio and the relative error for both models. We denoted by I_c the original clean image and by u the restored image. With this notations, we defined the SNR (signal to noise ratio) and the ReErr (relative error) as follows [9]:

$$SNR = 10log_{10}\frac{||I_c||_2^2}{||u - I_c||_2^2}, ReErr = \frac{||u - I_c||_2^2}{||I_c||_2^2}.$$

We summarized the results in table 1. From the quantitative comparison results shown in table 1 and from the computational results from figure 1(c)-(d) we can conclude that our model performs a better and faster denoising than the traditional RLO model for the same number of iterations. The parameters used for our model are $\alpha = 8$, $\lambda = 0.8$ and the number of iterations is $n = 50$.

Figure 2 shows a comparison of a reconstructed image obtained by using the proposed model with different $q(x)$. The test image is given in figure 1 (b). We compare the results of our model (2.3), when $q(x)$ is a function on the interval [1,2] with the case when $q(x)$ is a constant, either one or two. In our model, $q(x)$ varies from pixel to pixel and from iteration to iteration and provide better results than if $q(x)$ is fixed and does not vary in x and n. To illustrate this fact, we considered two cases for $q(x)$ constant:

1) $q(x) = 1$ and 2) $q(x) = 2$. In case 1), Figure 2 (c), the denoising is more slower and takes more iterations in order to obtain a satisfactory result. In case 2), Figure 2 (d), the denoising is faster and leads to a loss of the image details. As it can be seen in Figure 2 (b) and Table 2, the proposed model offers a better noise removal, being a combination of the TV-based and isotropic smoothing. The parameters used for the proposed model, for the experiments shown figure 2, are $\alpha = 3$, $\lambda = 0.3$ and the number of iterations is $n = 50$.

In the third experiment, we compare the results between the proposed model and RLO model (1.2), for an ultrasound image. The results are shown after 50 iterations and the parameters used for our model are $\alpha = 1$, $\lambda = 0.4$. We included the mean fields for our reconstructed image with the corresponding probabilities for the proposed model and the resulting minimized energy for each model. We can see from the energy plot in figure 3(h) that we reached an optimal solution after 50 iterations for the proposed model (2.3). The results show that our model performs a better and faster denoising, with feature preserving than the RLO model (1.2).

Figure 4 represents a comparison between our model (2.3) and model (1.8). Figure 4 (a) is the given image contaminated with multiplicative noise with mean zero and variance 0.1 and with contrast 17/60 on [0,255] gray scale. Figure 4 (b) represents the segmentation result $u(x)$ using our model, after 50 iterations, figure 4 (c)-(d) represent the mean fields of the segmentation result for our model. The parameters used for this experiment for our model are $\alpha = 7$, $\lambda = 0.7$. The results of model (1.8) are shown in figure 4 (e)-(j) after 50, respectively 1200 iterations. As we can see from table 3 and from the reconstructed image from figure 4 (b) , our model performs a better and faster segmentation than the model (1.8).

In experiment 5, we make a comparison between the segmentation results of the proposed model (2.3) and the model (1.8) for three different situations. These three initial images with different level of noise and different level of contrast, are represented in figure 5(a)-(c).

Figure 5(a) is an initial image with contrast 17/33 on [0,255] gray scale and noise of variance 0.03, figure 5(b) represents an initial image with contrast 17/60 on [0,255] gray scale and noise of variance 0.1 and the last initial image has contrast 17/138 on [0, 255] gray scale and noise of variance 0.2. The results are shown after 50 iterations. In figure 5 (j)-(l) we have shown the corresponding energies for the proposed model (2.3). As we can see from the comparison results, the proposed model performs well the segmentation for all the situations given above. From the experiments 4 and 5, we can conclude that the proposed model is faster, more robust to noise and contrast. For the proposed model, for these three different cases,we have used the parameters $\alpha = 8$, $\lambda = 0.8, \alpha = 7$, $\lambda = 0.7$, and respectively $\alpha = 5$, $\lambda = 0.5$. For the comparison model (1.8), we used the same initialization for all test images.

In the last experiment, we compare our model with model (1.8) for an thyroid ultrasound image. We have shown the final reconstructed result $u(x)$ and the corresponding mean fields $u_1(x), u_2(x)$ for both models. For our model, we used the parameters $\alpha = 1$, $\lambda = 0.4$. We have included the results for our model after 50 iterations and for the comparison model (1.8) after 50, respectively 1000 iterations. From this experiment we can conclude that our model performs a better segmentation for the same number of iterations.

All the experiments presented in this paper were performed on a Sony Vaio laptop with Intel Core 2 Duo T 6400, 2.0 GHz processor and 4GB memory (RAM).

Table 1: The SNR and ReErr for the synthetic image in Figure 1.

	Proposed model	RLO model
SNR	24.96	21.48
ReErr	0.00001	0.00005
CPU time	62.960000	153.381415

Table 2: The SNR and ReErr for synthetic image in Figure 2.

	q(x) variable	q(x) = 1	q(x) = 2
SNR	24.96	21.24	22.38
ReErr	0.00001	0.00005	0.00003

Table 3: The computing time for ultrasound thyroid image in Figure 3.

	Proposed model	RLO model
CPU time	39.362986	84.0805575

Table 4: The number of pixels per partition for synthetic image in Figure 4.

	Initial image	Proposed model 50 iterations	Vese model 50 iterations	Vese model 1200 iterations
U1	28847	28847	12467	28547
U2	28753	28753	45124	29053

5. Conclusions

The proposed model is a novel variational approach for simultaneous segmentation and denoising of images contaminated with multiplicative noise. By using the soft segmentation procedure and an energy functional with variable exponent for noise removal, the model becomes more robust to noise and performs a better segmentation.

The functional with variable exponent $\int_\Omega |\nabla u(x)|^{q(x)}$ provides a better noise removal with features preservation. It ensures the TV- based diffusion ($q(x) = 1$) along edges and Gaussian smoothing ($q(x) = 2$) in homogenous regions and, it employs anisotropic diffusion ($1 < q(x) < 2$) in regions in which the difference between noise and edge is difficult to distinguish.

We compared our model to some traditional models, for both real (ultrasound) and synthetic images and the computational results show the effectiveness of the proposed work.

6. References

References

[1] G. Aubert, J. Aujol, A variational approach to removing multiplicative noise, SIAM J. Appl. Math. 68, 925-946, 2008.

[2] E. Bae, J. Y., X. C. Tai, Simultaneous Convex Optimization of Regions and Region Parameters in Image Segmentation Models, UCLA CAM Report 11-83, 2011.

[3] X. Bresson, T. F. Chan, Non-local unsupervised variational image segmentation models, UCLA Cam report 08-67.

[4] E. S. Brown, T. F. Chan, and X. Bresson, A Convex Relaxation Method for a Class of Vector-valued Minimization Problems with Applications to Mumford-Shah Segmentation, UCLA CAM Report 10-43, 2010.

[5] V. Caselles, R. Kimmel and G. Sapiro, Geodesic active contours, Int.J. of Computer Vision, 1(1997), pp.61-79.

[6] T. F. Chan, L. Vese, Active contour without edges. IEEE Trans. on Image Processing, 10(1), pp. 266-277, 2001.

[7] G. Chung, L. Vese, Energy minimization based segmentation and denoising using a multilayer level set approach. Energy Minimization Methods in Computer Vision and Pattern Recognition, 3757(1), pp. 439-455, 2005.

[8] Y. Dong, T. Zeng, A convex variational model for restoring blurred images with multiplicative noise, UCLA CAM Report 12-23, 2012.

[9] R. C. Gonzales and R. E. Woods, Digital Imaging Processing, Pearson Prentice Hall, 2008.

[10] J. Huang, X. Yang, Y. Chen, A fast algorithm for global minimization of maximum likelihood based on ultrasound image segmentation. Inverse problems and imaging, 5(3) pp. 645-657, 2011.

[11] Y.-M. Huang, M.K. Ng, Y-W Wen, A new total variation method for multiplicative noise removal, SIAM J. Imaging Sci 2(1) pp. 20-40, 2009.

[12] Z. Jin, X. Yang. Analysis of a new variational model for multiplicative noise removal. J. Math. Anal. Appl. 362 (2010) pp. 415-426

[13] Z. Jin, X. Yang, A variational model to remove the multiplicative noise in ultrasound images. J. Math. Imaging Vis (2011) 39 pp.62-74.

[14] Y. Jung, S. Kang, J. Shen, Multiphase image segmentation via Modica-Mortola phase transition. SIAM Applied Math., 67(1), pp. 1213-1232, 2007.

[15] P. Kornprobst, R. Deriche, G. Aubert, Image sequence analysis via partial differential equations. J. Math. Imaging Vis. 11(1): 5-26, 1999.

[16] K. Krissian, R. Kikinis, C.-F. Westin, K. Vosburgh, Speckle-constrained filtering of ultrasound images, IEEE Computer Society Conference on Computer Vision and Pattern Recognition (CVPR'05) - Volume 2, pp.547-552, 2005.

[17] T. Le, L. Vese, Additive and multiplicative piecewise-smooth segmentation models in a functional minimization approach. Interpolation Theory and Applications: A conference in honor of Michael Cwikel, Miami, Florida, Editors: Laura De Carli and Mario Milman, Comtemporay Mathematics, vol. 445, pp. 207-223, 2007.

[18] M. Lysaker, A. Lundervold, X. C. Tai, Noise removal using fourth-order partial differential equation with application to medical MRI in space and time. IEEE Trans. Image Process. 12 (12), pp. 1579-1590, 2003.

[19] D. Mumford and J. Shah, Optimal approximations by piecewise smooth functions and associated variational problems, Comm. on Pure and Applied Math., 49(1989), pp. 577-685.

[20] N. Paragios and R. Deriche, Geodesic active regions for supervised texture segmentation, Proceedings of International Conference on Computer Vision, 1999, pp.22-25.

[21] I. Posirca, Y. Chen, C. Barcelos, A Stochastic Variational PDE Model for Soft Mumford-Shah Segmentation, Journal of Mathematical Analysis and Applications 384 (2011), pp. 104-114.

[22] L. Rudin, S. Osher, E. Fatemi, Nonlinear total variation based noise removal algorithms. Physica D 60 (1992) pp. 259-268.

[23] L. I. Rudin, P. L. Lions, S. Osher, Multiplicative denoising and deblurring: Theory and algorithms, in: S.Osher, N. Paragios (Eds), Geometric Level Sets in Imaging, Vision, and Graphics, Springer, 2003, pp. 103-119.

[24] A. Sarti, C. Corsi, E. Mazzini, Maximum likelihood segmentation of ultrasound images with Rayleigh distribution. IEEE Trans. Ultrasonics Ferroelectrics and Frequency Control, 52 (2005), pp.947-960.

[25] J. Shen, A stochastic variational model for soft Mumford-Shah segmentation, International Journal of Biomedical Imaging, Volume 2006, pp. 1-14.

[26] A. Tsai, A. Yezzi, A. S. Willsky, Curve Evolution Implementation of the MumfordShah Functional for Image Segmentation, Denoising, Interpolation, and Magnification. IEEE Transactions on Image Processing, 10(8), pp. 1169-1186, 2001.

[27] L. Vese, T. Chan, A multiphase level set framework for image segmentation using the Mumford and Shah model. Int J.of Comp. Vision 50(3), pp. 271-293, 2002.

[28] S. C. Zhu, A. Yuille, Region competition : unifying snakes, region growing, and Bayes/ MDL for multi-band image segmentation. IEEE Trans. Pattern Anal. Machine Intell., 18(9): 884-900, 1996.
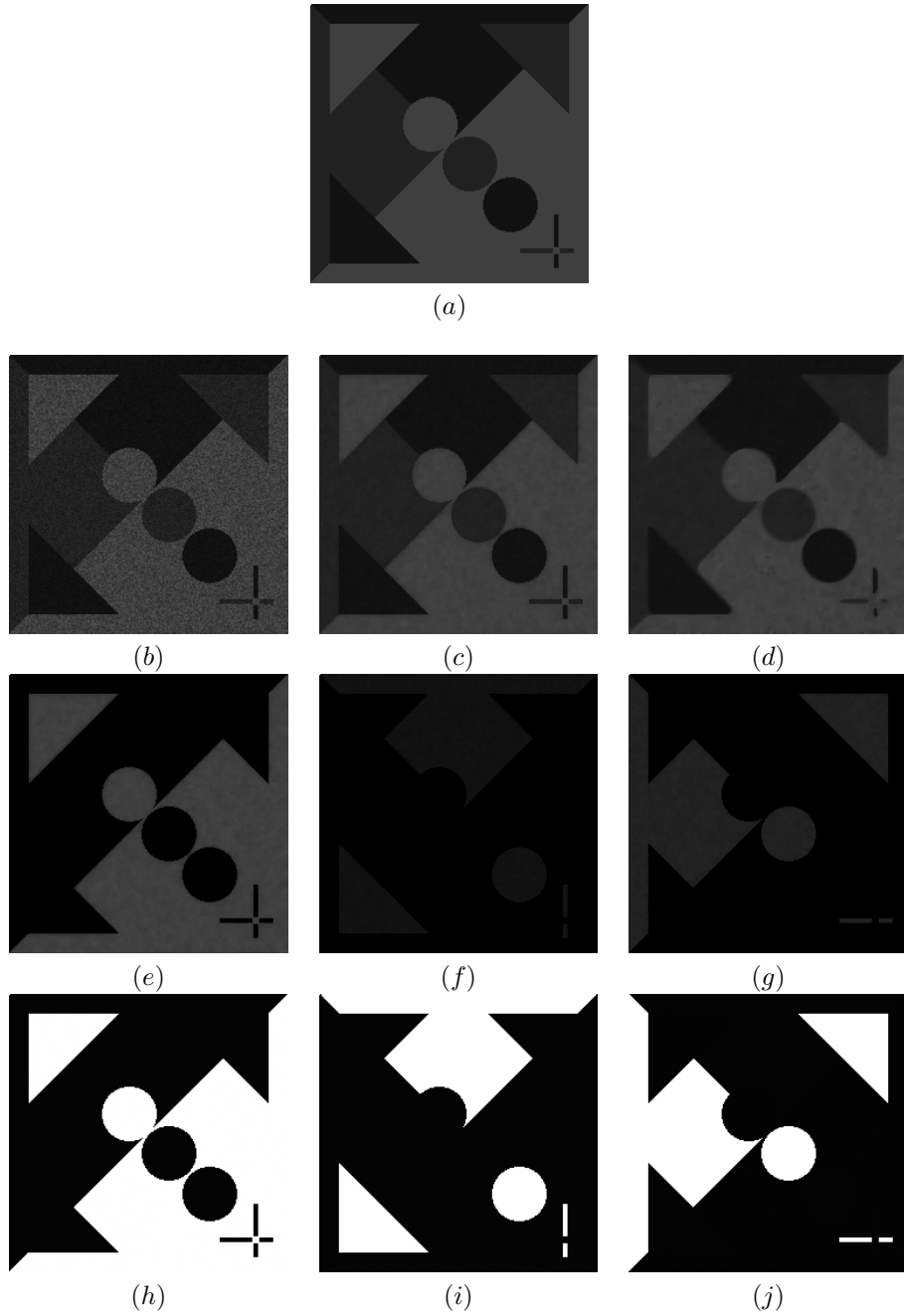
Figure 1: (a) Synthetic image. (b) Synthetic image with noise. (c) The denoised image result obtained by using the proposed model.
(d) The denoised image result obtained by using the RLO model (1.2).
(e),(f),(g) The mean fields $u_1(x), u_2(x), u_3(x)$ for the result (c).
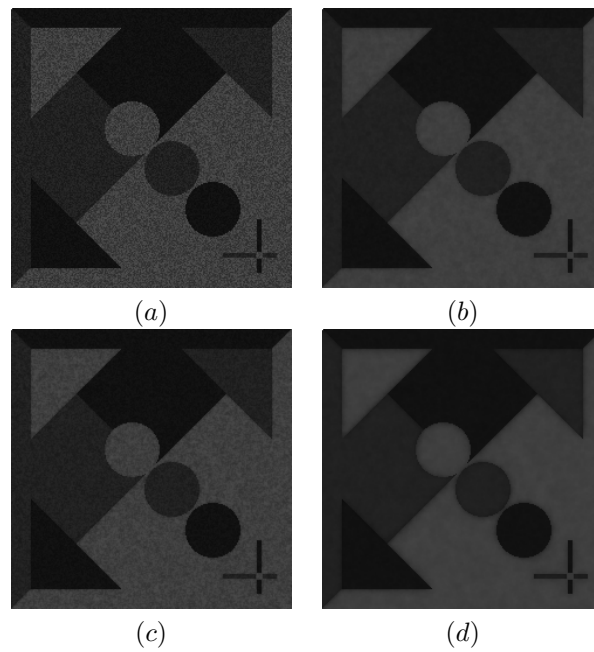(h),(i),(j) The corresponding probabilities $p_1(x), p_2(x), p_3(x)$ for our model (2.3).

(a) (b)

(c) (d)

Figure 2: Comparison on $q(x)$: (a) Synthetic image corrupted with multiplicative noise.
(b) The reconstructed image using $q(x)$ variable.
(c) The reconstructed image using $q(x) = 1$ fixed in our model.
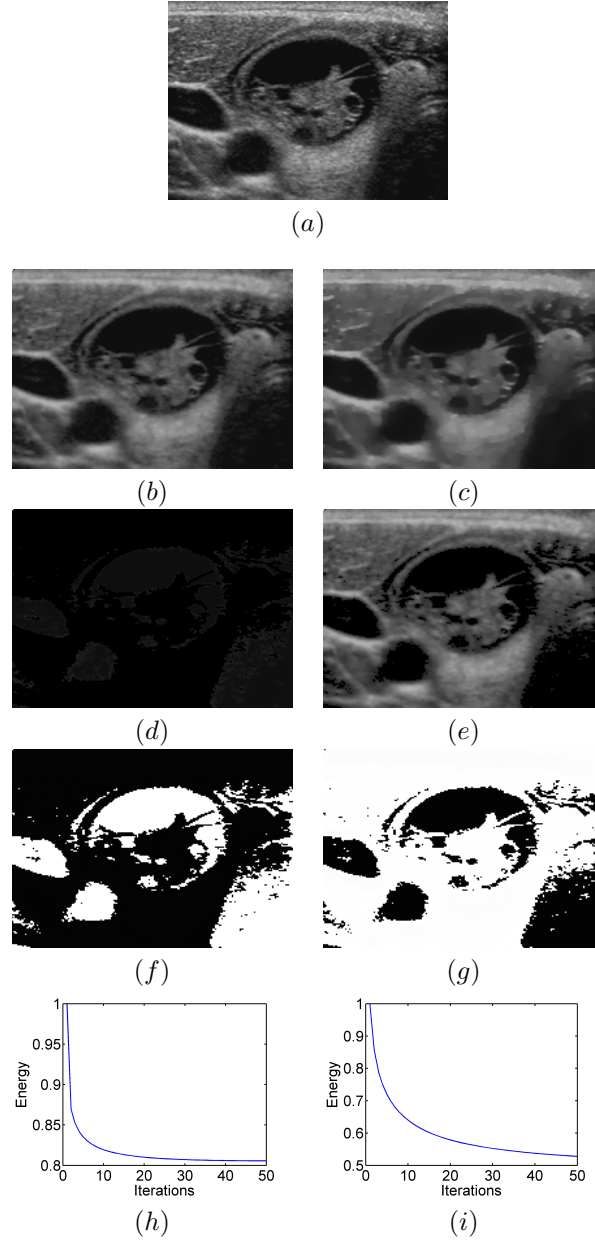(d) The reconstructed image using $q(x) = 2$ fixed in our model.

Figure 3: (a) Ultrasound thyroid with noise.
(b) The denoised image obtained by using the proposed model (2.3).
(c) The denoised image result using the RLO model (1.2).
(d)-(e) The mean fields $u_1(x), u_2(x)$ of the patterns for model (2.3).
(f)-(g) The corresponding probabilities $p_1(x), p_2(x)$ for model (2.3).
(h)-(i) The normalized energy versus iterations for the proposed model (2.3) and for RLO model (1.2).

(a)

(b)

(c)

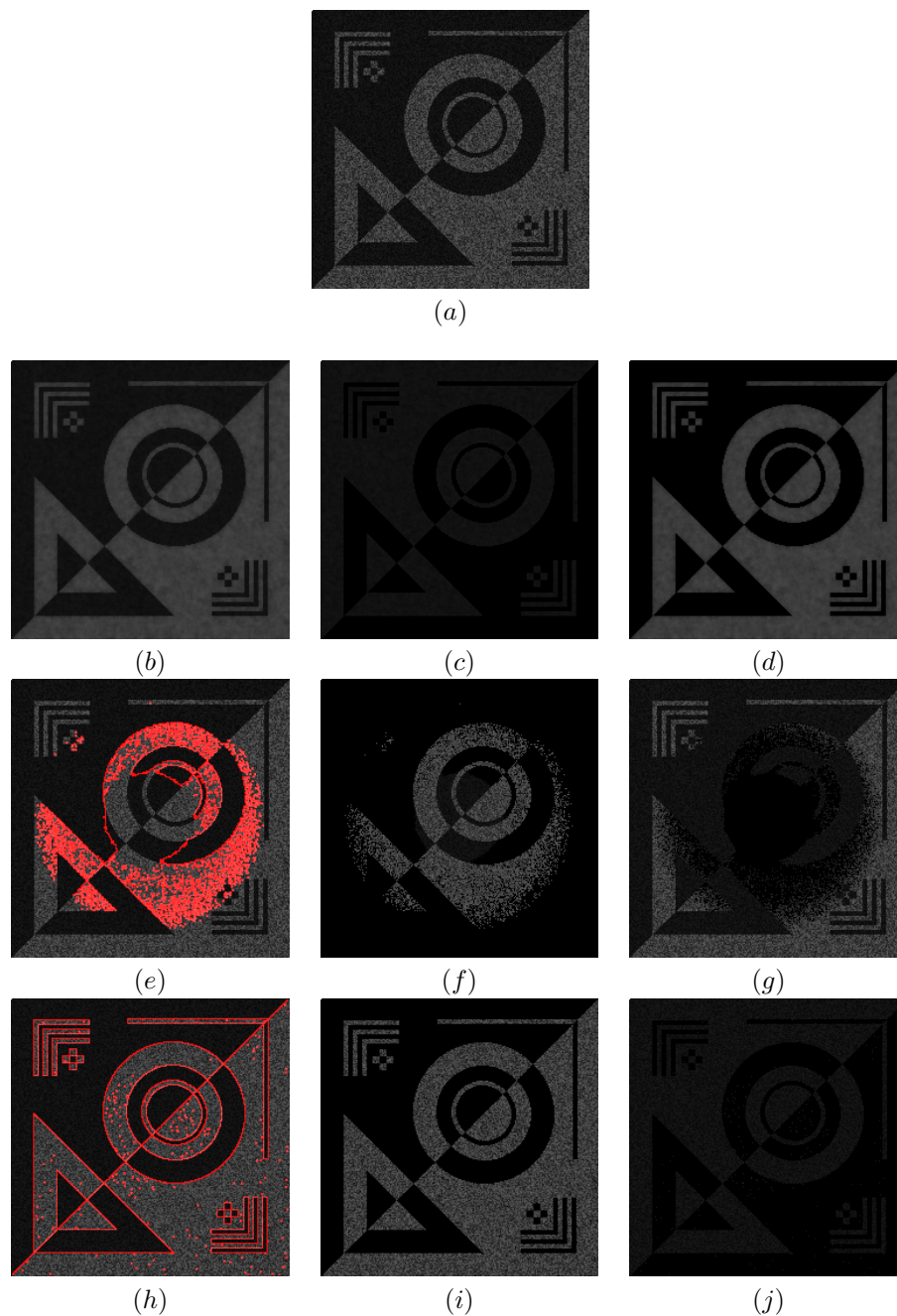(d)

(e)

(f)

(g)

(h)

(i)

(j)

Figure 4: (a) Synthetic image with noise. (b) Segmentation result using the proposed model (2.3) after 50 iterations.
(c)-(d) The mean fields $u_1(x), u_2(x)$ of the segmentation result (b).
(e) Segmentation result using model (1.8) after 50 iterations.
(f)-(g) The mean fields $u_1(x), u_2(x)$ of the patterns for model (1.8) after 50 iterations.
(h) Segmentation result using model (1.8) after 1200 iterations.
(i)-(j) The mean fields $u_1(x), u_2(x)$ of the patterns for model (1.8) after 1200 iterations.
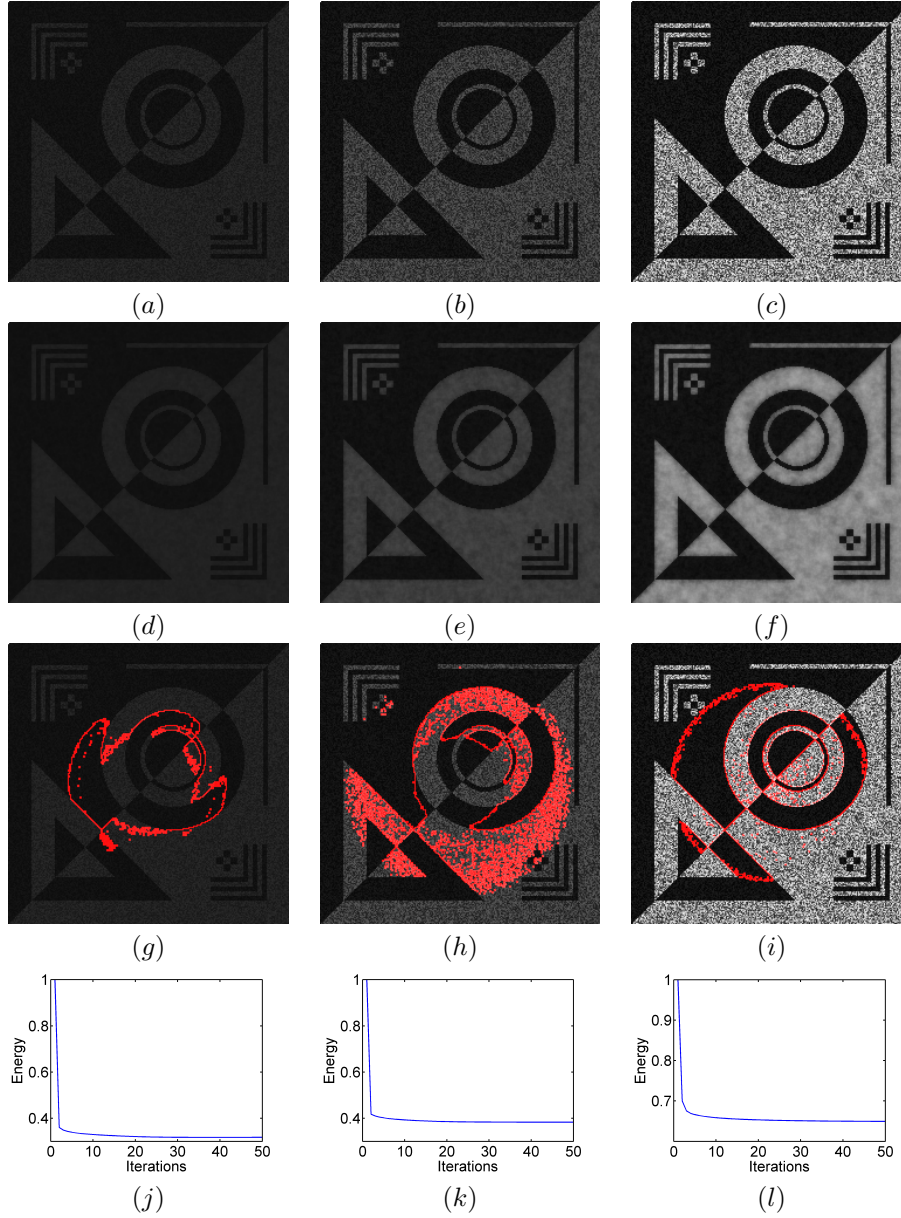
Figure 5: (a)-(b)-(c) Initial images with different level of contrast and different level of noise. (d)-(e)-(f) The corresponding segmentation results using the proposed model (2.3). (g)-(h)-(i) The corresponding segmentation results using model (1.8). (j)-(k)-(l) The normalized energy versus iterations for the proposed model (2.3).

(a)

(b) (c) (d)

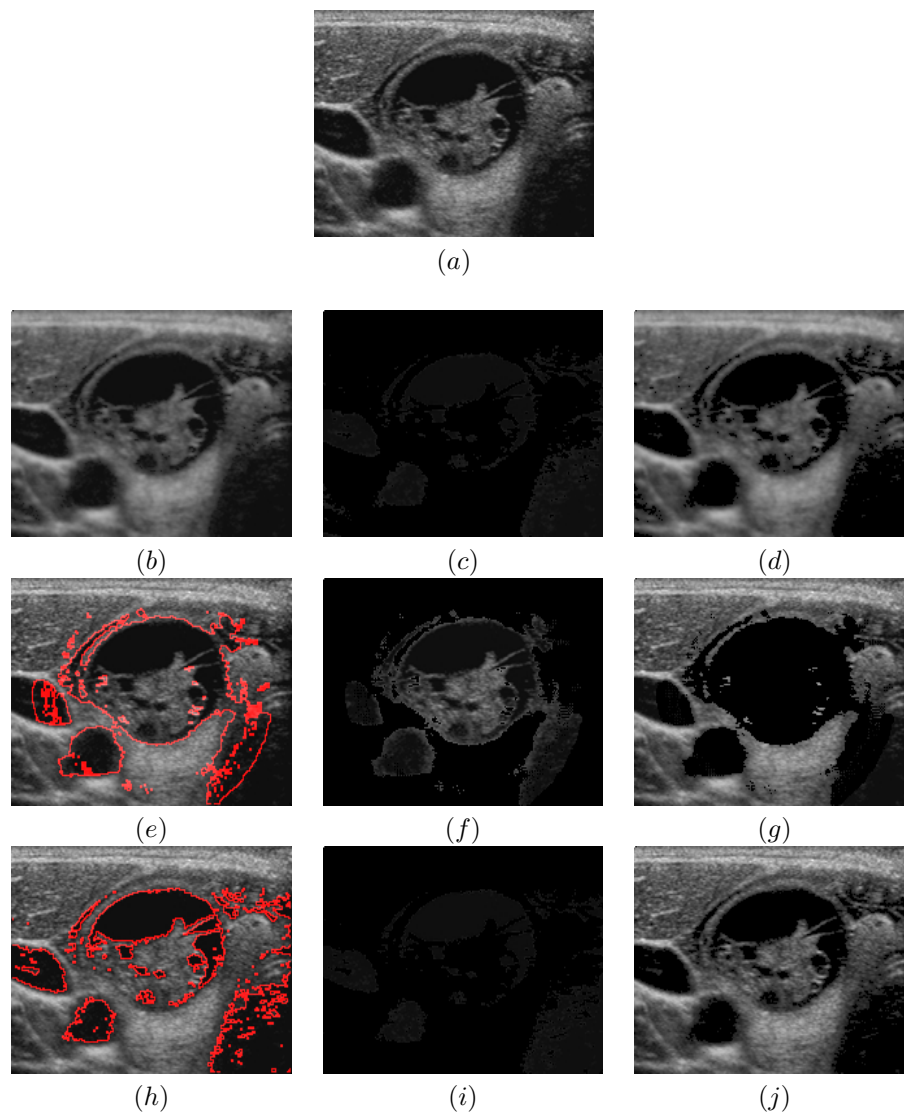(e) (f) (g)

(h) (i) (j)

Figure 6: (a) Ultrasound thyroid with noise. (b) Segmentation result using the proposed model (2.3).
(c)-(d) The mean fields $u_1(x), u_2(x)$ of the patterns for our model.
(e) Segmentation result using model (1.8) after 50 iterations.
(f)-(g) The corresponding mean fields $u_1(x), u_2(x)$ for (e).
(h) Segmentation result using model (1.8) after 1000 iterations.
(i)-(j) The corresponding mean fields $u_1(x), u_2(x)$ for (h).